Major Pleistocene stages in a carbon perspective: The South China Sea record and its global comparison

Pinxian Wang, Jun Tian, Xinrong Cheng, Chuanlian Liu, and Jian Xu
Laboratory of Marine Geology, Tongji University, Shanghai, China

Received 25 November 2003; revised 3 July 2004; accepted 28 July 2004; published 13 October 2004.

[1] Carbon isotope sequences at Ocean Drilling Program Site 1143, South China Sea, reveal a long-term cyclicity of ~500 kyr that is superimposed on the glacial cycles and is present in long $\delta^{13}C$ sequences from all oceans. The Quaternary $\delta^{13}C$ record is punctuated by four $\delta^{13}C$ maximum events: $\delta^{13}C$max-I, which began in marine isotope stage (MIS) 3 around 50–60 kyr ago, $\delta^{13}C$max-II (MIS 13, 0.47–0.53 Ma), $\delta^{13}C$max-III (MIS 27–29, 0.97–1.04 Ma) and $\delta^{13}C$max-VI (MIS 53–57, 1.55–1.65 Ma). As the same cyclicity is also found in carbonate curves, the $\delta^{13}C$max events must denote major reorganization in the carbon reservoir of the global ocean. They also are associated with major changes in glacial cyclicity, such as the Mid-Brunhes Event following $\delta^{13}C$max-II and the Mid-Pleistocene Revolution following $\delta^{13}C$max-III, which in turn were associated with expansion of the ice sheets. From a carbon perspective, therefore, the Quaternary period has passed through three major stages, and each appears to represent a further step in ice cap development. *INDEX TERMS:* 1615 Global Change: Biogeochemical processes (4805); 3030 Marine Geology and Geophysics: Micropaleontology; 4267 Oceanography: General: Paleoceanography; 4805 Oceanography: Biological and Chemical: Biogeochemical cycles (1615); 4806 Oceanography: Biological and Chemical: Carbon cycling; *KEYWORDS:* long-term cyclicity, carbon isotope, South China Sea

Citation: Wang, P., J. Tian, X. Cheng, C. Liu, and J. Xu (2004), Major Pleistocene stages in a carbon perspective: The South China Sea record and its global comparison, *Paleoceanography*, *19*, PA4005, doi:10.1029/2003PA000991.

1. Introduction

[2] The Quaternary is a period of glaciation. Alternating growth and decay of polar ice sheets, regulated by orbital forcing, characterize Quaternary history, and the resulting oxygen isotope variations in marine sediments provide the best basis for stratigraphic correlation of Quaternary records. Recently, the concept of glacial dominance of Quaternary history was challenged by the discovery that changes of CO_2 lead changes of ice volume [*Shackleton*, 2000], and it is becoming apparent that the global carbon cycle has its own response to orbital forcing and its own history, which does not originate simply from glacial changes [*Keigwin and Boyle*, 1985; *Crowley*, 1995].

[3] The last decade has yielded a number of long sequences of carbon isotope and carbonate records from deep-sea sediments covering the entire Quaternary, which reveal carbon cycle history and allow us to identify major stages from a carbon perspective. This paper proposes three major stages in carbon isotope and carbonate records of the Quaternary, on the basis of our recent studies on ODP Site 1143 from the southern South China Sea (SCS) and its comparison with records from other sites in the global ocean (locations, Figure 1).

2. Material and Methods

[4] ODP Site 1143 is located 9°21.72′N, 113°17.11′E, in the Nansha or Dangerous Grounds area of the southern SCS, at a water depth of 2772 m (Figure 1). Three holes were drilled at the site, with a coring depth of 510 m, providing a history over the past 12 Myr [*Wang et al.*, 2000]. The upper 190 m consists mostly of greenish gray clayey sediments rich in calcareous nannofossils and foraminifers and covers the last 5.0 Myr, according to biostratigraphic, paleomagnetic and isotopic data [*Wang et al.*, 2001; *Tian et al.*, 2002]. This upper section was sampled mostly at 10-cm intervals and analyzed for oxygen and carbon isotopes, equivalent to a time resolution of about 2 kyr. From each sample, benthic foraminifers *Cibicidoides wuellerstorfi* or *Uvigerina* spp., and planktonic foraminifers *Globigerinoides ruber* were analyzed in the Laboratory of Marine Geology, Tongji University, except for a few samples where no sufficient foraminiferal tests could be picked out. The same set of samples from the uppermost 95 m, covering the last 2.0 Myr, was quantitatively analyzed for microfossils, including planktonic foraminifers [*Xu et al.*, 2004] and coccoliths using techniques described elsewhere [*Liu et al.*, 2002], for reconstructing upper ocean conditions in the Pleistocene. Because of the significant dilution effect of terrigenous material, the coarse fraction of bulk samples (>63 μm), foraminiferal abundance and fragmentation were used to indicate carbonate preservation and production. To address the question of carbon cycle changes in the Pleistocene, results from Site 1143 were compared with available sequences from other ODP sites in various oceans, which form the basis of the present study.

3. Record From ODP Site 1143

[5] Figure 2 shows high-resolution $\delta^{13}C$ records for the last 5 Myr from Site 1143 based on planktonic and benthic

0883-8305/04/2003PA000991$12.00

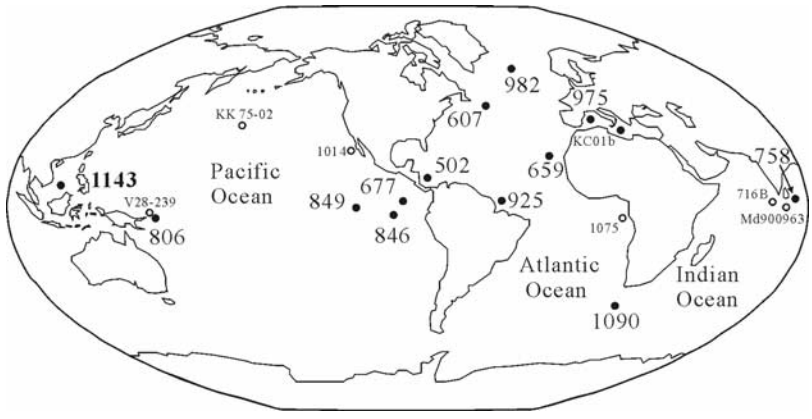

Figure 1. Locations of ODP Site 1143 in the southern South China Sea and other ODP sites used for comparison. Heavy numerals and solid circles indicate sites used in Table 1 and Figures 6–7.

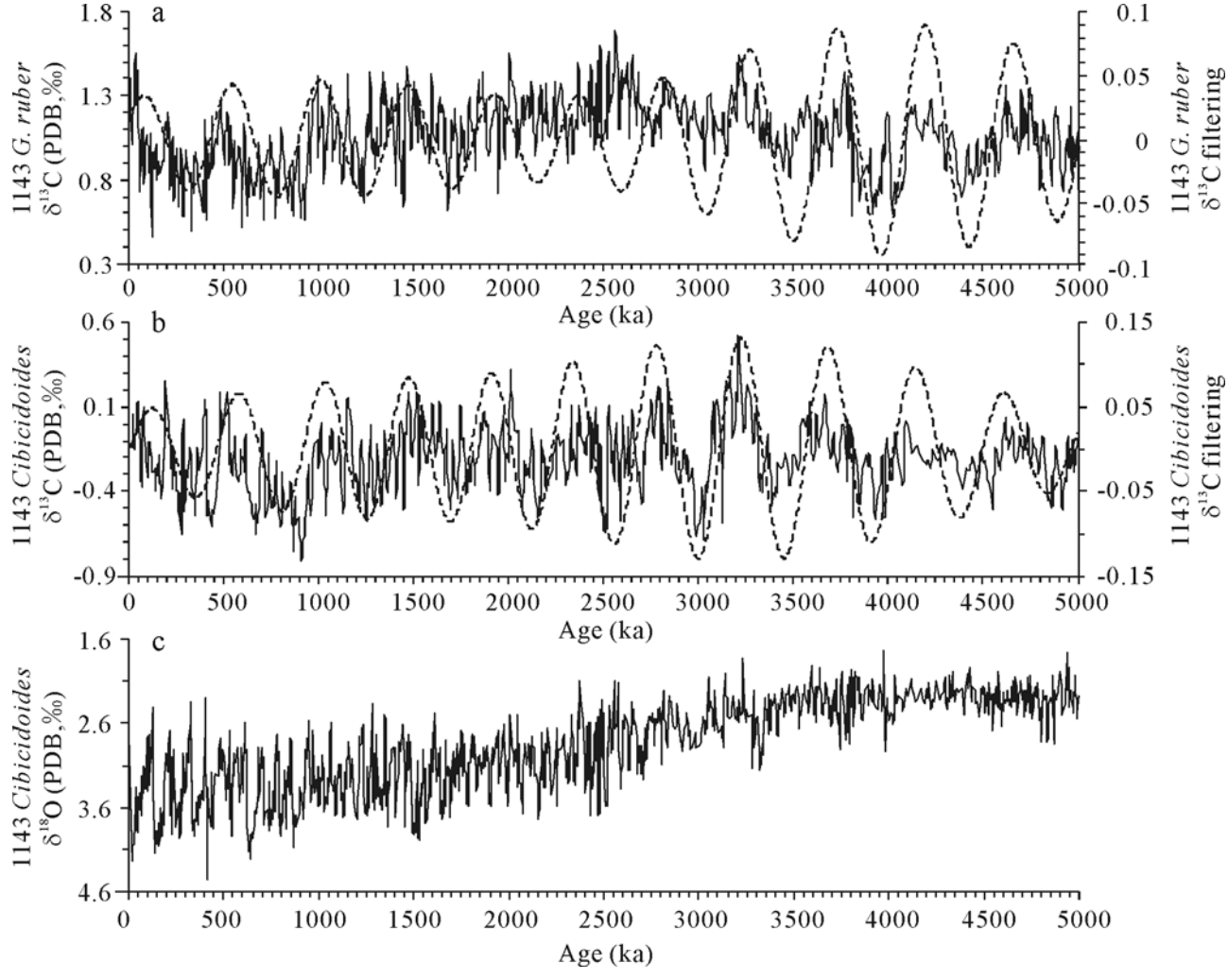

Figure 2. The 5.0 Myr isotope records from ODP Site 1143. (a) $\delta^{13}C$ of *Globigerinoides ruber* after 5-point Gaussian smoothing (solid line). (b) $\delta^{13}C$ of *Cibicidoides* spp. after 5-point Gaussian smoothing (solid line). (c) $\delta^{18}O$ of *Cibicidoides* spp. Dashed lines in Figures 2a and 2b denote the Gaussian filtering of $\delta^{13}C$ records, with a central frequency of 0.0022 kyr^{-1} and bandwidth of 0.00022 kyr^{-1}.

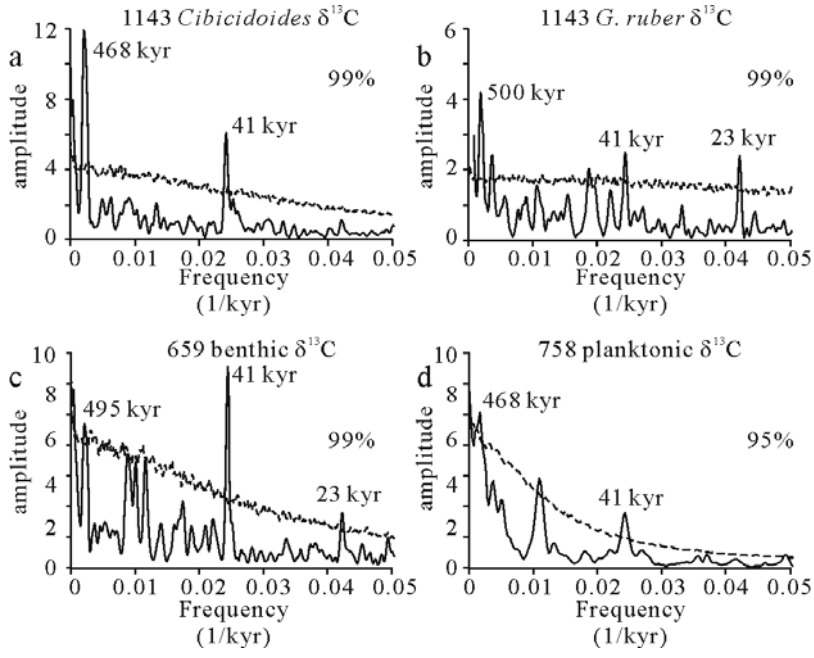

Figure 3. Bias-corrected spectrum of (a) ODP Site 1143 *Cibicidoides* $\delta^{13}C$ (0–5 Ma), (b) ODP Site 1143 *G. ruber* $\delta^{13}C$ (0–5 Ma), (c) ODP Site 659 benthic $\delta^{13}C$ (0–5 Ma), and (d) ODP Site 758 planktonic $\delta^{13}C$ (0–2.6 Ma). Dashed lines indicate false-alarm level (99% and 95‰). The program "REDFIT" was used to perform the spectral analyses [*Schulz and Mudelsee*, 2002].

foraminifers (*Globigerinoides ruber* and *Cibicidoides* spp., respectively), together with $\delta^{18}O$ of *Cibicidoides* spp.

[6] The age model is based on the benthic oxygen isotope record tuned to obliquity and precession using the *Laskar* [1990] (1, 0) astronomical solution and an automatic tuning method [*Yu and Ding*, 1998], supported by biostratigraphic and magnetostratigraphic data [*Tian et al.*, 2002]. A distinctive feature of the $\delta^{13}C$ curves is the occurrence of long-period variations that are superimposed on the orbital (Milankovitch) periods that are used in tuning the age model [*Wang et al.*, 2003]. To reveal the long-term period, we first applied Gaussian filtering to each of the $\delta^{13}C$ records, with a central frequency of 0.0022 kyr^{-1} and bandwidth of 0.00022 kyr^{-1}. The filtering results show the cyclic variations of periodic components of $\delta^{13}C$ ranging from 400 kyr to 500 kyr for the past 5 Myr (dashed lines in Figure 2). Then we proceeded to spectral analysis. However, spectra of paleoclimatic time series frequently show a continuous decrease of spectral amplitude with increasing frequency (red noise) [*Hasselmann*, 1976]. To minimize the drawbacks, we utilized a computer program "REDFIT" developed by *Schulz and Mudelsee* [2002] to perform the spectral analyses. Aside from periodic variations of 100 kyr, 41 kyr and 23 kyr cycles, the spectral analyses also revealed significant periodicity close to 500 kyr above the 99% false alarm level (Figures 3a and 3b).

[7] Visual inspection of the bandpass filter in Figure 2 shows the changing length of the long-term period from Pliocene to the Pleistocene. This observation is confirmed by the low-frequency continuous wavelet transform analysis (CWT) of the benthic $\delta^{13}C$ record from Site 1143 (Figure 4a). Continuous wavelet transform is widely used to analyze time series that contain nonstationary power at many different frequencies [*Torrence and Compo*, 1998]. The modulus of the low-frequency components around 400–500 kyr is fairly prominent, but its peak or "ridge" (white line in Figure 4) declined with age, being close to 413 kyr in the Pliocene but extending to ~500 kyr in the Pleistocene.

[8] All of the applied statistical analyses thus show a period of ~500 kyr in both the benthic and planktonic $\delta^{13}C$ records over the last 2 Myr. These longer periods culminate in $\delta^{13}C$ maxima at around 0–60 kyr (MIS 1–3), 0.47–0.53 Ma (MIS 13), 0.97–1.04 Ma (MIS 27–29) and 1.55–1.65 Ma (MIS 53–57). There are other maxima (e.g., at ~200 and 700 kyr in the benthic record) but these four broad peaks are crests of the dominant long-period cycles. For convenience in further discussion, we will label the four events in order of increasing age as $\delta^{13}C$max-I, $\delta^{13}C$max-II, $\delta^{13}C$max-III and $\delta^{13}C$max-IV (Figure 5).

[9] Later in the paper we argue that the $\delta^{13}C$max peaks are expressions of widespread changes in the global carbon cycle, that interlock with major changes in the glacial cycles. However, first we draw attention to other features of the record from Site 1143. 500 kyr cycles also are apparent in almost all of the micropaleontological records and in carbonate preservation (Figure 5). The coarse fraction percent (>63 μm) and foraminiferal abundance (specimens per gram sediment) curves (Figures 5b and 5c) nearly mirror the benthic $\delta^{13}C$ curve (Figure 5a), and the foraminiferal fragmentation percent (Figure 5d) varies in broad accordance with $\delta^{13}C$, suggesting close ties between the carbon isotope and carbonate system in the ocean. Interestingly, the long $\delta^{13}C$ cycles also find expression in the plankton community, with the minimal percentages of some

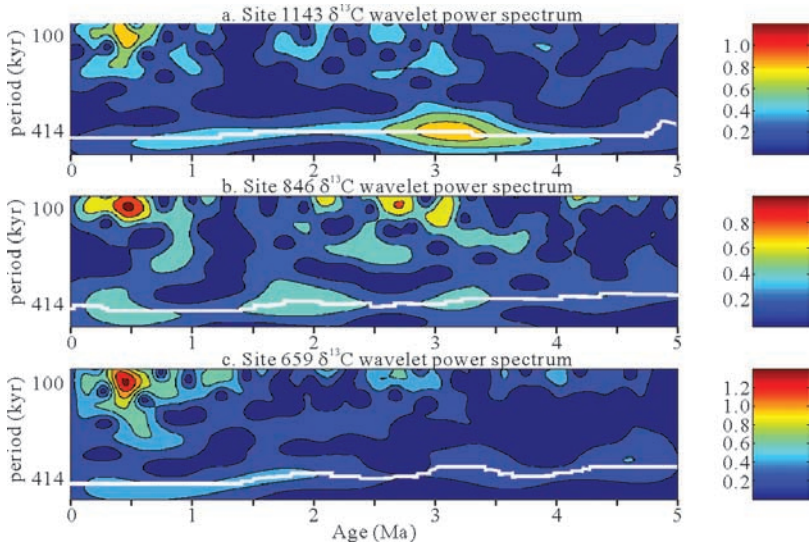

Figure 4. Modulus of the continuous wavelet transform of benthic $\delta^{13}C$ from (a) ODP site 1143, (b) ODP site 846, and (c) ODP site 659. The white lines are the ridges of the low-frequency variability centered around 1/400–1/500 kyr. The right color bar denotes the modulus density, with higher values indicating higher density.

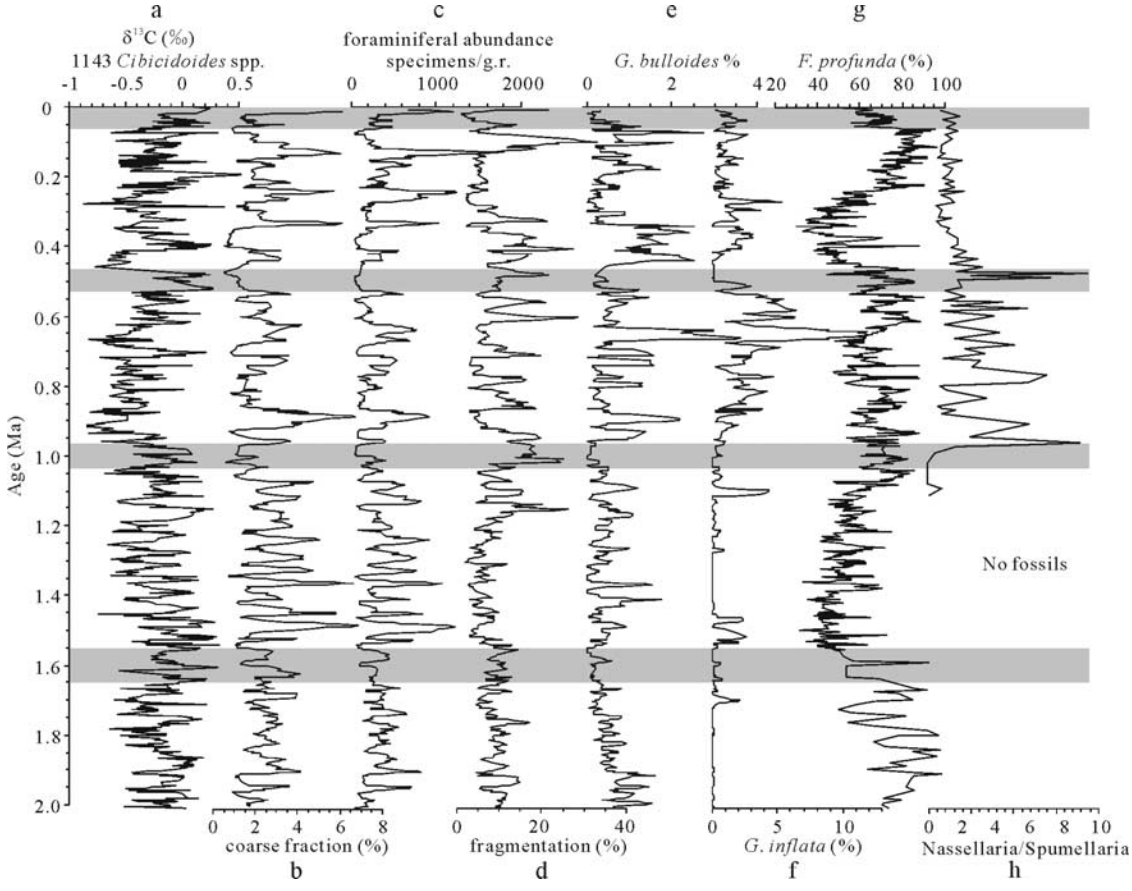

Figure 5. Micropaleontological and geochemical records of ODP Site 1143 over the last 2 Myr. (a) $\delta^{13}C$ of *Cibicidoides* spp. (‰), (b) coarse fraction (>150 μm) percent, (c) foraminiferal abundance (specimens/g), (d) foraminiferal fragmentation, (e) *Globigerina bulloides* percent, (f) *Globorotalia inflate* percent, (g) *Florisphaera profunda* percent, and (h) ratio of radiolarian groups Nassellaria/Spumellaria [*Yang et al.*, 2002]. Gray bars denote $\delta^{13}C$max.

Table 1. Carbon Isotope Sequences Over the Last 5 Myr From the World Ocean[a]

Site	Location	Water Depth, m	Time Span, Myr	Sedimentation Rate, cm/kyr	Resolution, kyr	Foraminifera	Reference
			West Pacific Ocean				
806	0°19′N 159°22′E	2534	2.1	2.1	4–5	P	*Schmidt et al.* [1993]
1143	9°22′N 113°17′E	2772	4.85	3.9	2.6 (P) 2.8 (B)	P, B	this paper
			Indian Ocean				
758	5°23′N 90°21′E	2925	3.6	1.5	~7	P, B	*Chen et al.* [1995] *Farrell and Janecek* [1991]
			East Pacific Ocean				
677	1°12′N 83°44′W	3461	2.6	4.5	2.2	P, B	*Shackleton et al.* [1990]
846	3°06′S 90°49′W	3296	6	4.2	2.5	B	*Shackleton et al.* [1995]
849	0°11′N 110°31′W	3851	5	2.8	~4	B	*Mix et al.* [1995]
			North Atlantic Ocean				
982	57°31′N 15°52′W	1134	3.2	2.2	2.5	B	*Venz and Hodell* [2002]
607	41°00′N 32°58′W	3427	2.8	4.5	~4	B	*Raymo et al.* [1989]
659	18°05′N 21°02′W	3070	5	2.9	~4	B	*Tiedemann et al.* [1994]
502	11°29′N 79°23′W	3051	1.9	2.0	5.8	P	*Prell* [1982]
925	4°12′N 43°29′W	3041	2.6	3.2	3.1	B	*Bickert et al.* [1997]
975	38°54′N 4°41′E	2415	1.9	6.8	3.0	P	*Pierre et al.* [1999]
			South Atlantic Ocean				
1090	42°55′S 8°54′E	3702	2.9	2.0	2–4	P	*Venz and Hodell* [2002]

[a]Abbreviations are as follows: F, foraminifera; B, benthic; P, planktonic.

planktonic foraminifers, such as *Globigerina bulloides* and *Globorotalia inflata* (Figures 5e and 5f), corresponding to δ^{13}Cmax. In the nannofossil record, percent abundance of thermocline-dwelling nannoplankton *Florisphaera profunda* shows peaks close to δ^{13}Cmax-I, δ^{13}Cmax-II and δ^{13}Cmax-III (Figure 5g). These *F. profunda* peaks also coincide with minima in the coarse (>63 μm) sediment fraction (Figure 5b). A similar pattern occurs at ODP Site 1146, northern South China Sea; in addition at Site 1146, the mixed layer nannoplankton small *Gephyrocapsa* shows an opposite trend (X. Su, personal communication, 2002). The 500 kyr cycles in the last million years can also be observed in a radiolarian record at Site 1143, as expressed in the Nassellaria/Spumellaria ratio (Figure 5h).

[10] Although we consider that the δ^{13}C record from Site 1143 shows that long-period changes occur within the global carbon system, the system obviously is complex because closer inspection of Figures 2 and 4 reveals that the δ^{13}Cmax episodes differ in detail. The timing of δ^{13}C peaks, for example, differs between the foraminifera and nannofossil curves [*Liu et al.*, 2002]. For the moment, we look to evaluate whether long period variations found in the South China Sea also occurred in other oceans.

4. Comparison of Site 1143 With Other Long Records

[11] To ascertain whether the δ^{13}C maxima seen at Site 1143 were local or global, we compare the Site 1143 record with long-term δ^{13}C sequences from other long-record sites over the global ocean. Only sequences exceeding 2 Myr in length and higher than 5–6 kyr in resolution have been taken for comparison. In total, 12 sites from various oceans are used (Figure 1; Table 1).

[12] The North Atlantic turns out to be the richest ocean in number of relevant isotopic sequences. Figure 6 shows δ^{13}C curves at six sites from the North Atlantic and the Mediterranean, mostly with $CaCO_3$% or coarse fraction curves. The Atlantic is the only ocean where the compared sites are distributed from high (ODP Sites 982, 607) to low latitudes (ODP sites 659, 925 and DSDP Site 502), plus a site from the Western Mediterranean (Site 975) (see Table 1 for references). The curves in Figure 6 are adopted from the original publications, except for Site 502 where the age model has been revised to follow that of *Shackleton et al.* [1990].

[13] All the δ^{13}C curves in Figure 6 display the same general long term trend as at Site 1143, yet the Atlantic records show much more significant amplitude of downcore fluctuations. The total range of benthic δ^{13}C variations is about 1.5‰ at Site 1143 (Figure 2b), but reaches 2‰ in benthic δ^{13}C sequences from the North Atlantic (Figures 6b, 6d, 6f, and 6h). Noticeable is the similar trend in both the last two cycles between δ^{13}C max III and II, and between δ^{13}C max II and I: each cycle starts with the largest glacial/interglacial excursion of δ^{13}C, then the amplitude diminishes upward until the next δ^{13}C max episode (Figure 6). This is less clear in planktonic records from the Mediterranean (Figure 6j) and Atlantic (Figure 6k). Both spectral analysis and wavelet analysis of the benthic δ^{13}C sequence from Site 659 show similar long-term periods throughout the 5 Myr record (Figures 3c and 4c).

[14] Unlike δ^{13}C, the carbonate records in the North Atlantic vary significantly with the site location. For example, at ODP Site 925 on the Ceara Rise off the Amazon estuary, the minimal values of $CaCO_3$% are relatively stable (Figure 6e) [*Harris et al.*, 1997], whereas for Site 607 in the north far away from river input, the $CaCO_3$% curve shows relatively stable maximal values (Figure 6g) [*Ruddiman et al.*, 1989; *Raymo et al.*, 1989]. Regardless of the differences, nearly all records show long-term cycles similar to those in δ^{13}C, with diminished amplitude of variations at the

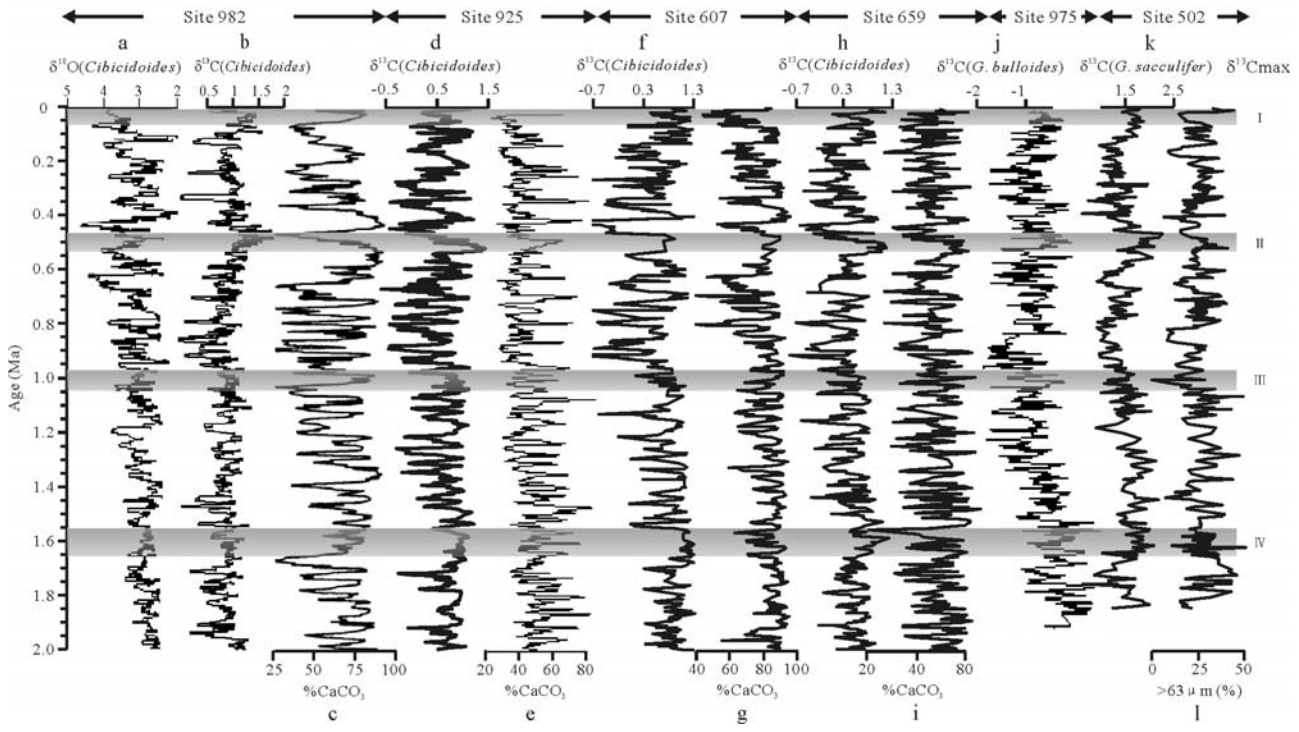

Figure 6. Carbon isotope and carbonate records over the last 2 Myr in the North Atlantic Ocean. Rockall Plateau, ODP 982: (a) $\delta^{18}O$ of *Cibicidoides*, (b) $\delta^{13}C$ of *Cibicidoides* [*Venz and Hodell*, 2002], and (c) carbonate percent based on reflectance spectroscopy [*Ortiz et al.*, 1999]. Ceara Rise, ODP 925: (d) $\delta^{13}C$ of *Cibicidoides* [*Bickert et al.*, 1997] and (e) carbonate percent based on reflectance spectroscopy and magnetic susceptibility [*Harris et al.*, 1997]. Western flank of Mid-Atlantic Ridge, ODP 607: (f) $\delta^{13}C$ of *Cibicidoides* and (g) carbonate percent [*Ruddiman et al.*, 1989; *Raymo et al.*, 1989]. Eastern equatorial, ODP 659: (h) $\delta^{13}C$ of *Cibicidoides* [*Tiedemann et al.*, 1994] and (i) carbonate percent [*Tiedemann et al.*,1994]. Western Mediterranean, ODP 975: (j) $\delta^{13}C$ of *G. bulloides* [*Pierre et al.*, 1999]. Caribbean, DSDP 502: (k) $\delta^{13}C$ of *G. sacculifer* and (l) coarse fraction (>63 μm, %) [*Prell*, 1982].

$\delta^{13}C$ maxima (Figures 6), suggesting a common mechanism causing the carbon isotope and carbonate changes.

[15] From other oceans, four sites in the tropical Pacific were found to be comparable with Site 1143 in time length and resolution (Figure 1; Table 1). Again, the planktonic $\delta^{13}C$ at Site 806 (Figure 7g) is similar to that at Site 1143 (Figure 2a), and the coarse fraction percent curve (Figure 7f) [*Yasuda et al.*, 1993] also shares the common features of the long 500-kyr cycles and minimal values at $\delta^{13}C$max. The three benthic $\delta^{13}C$ records from the Eastern Pacific are very close to each other in general trend and in details (Figures 7b, 7d, and 7e), with the total range of down-core variations less than 1.5‰, subdued relative to that in the Atlantic (2‰), but closer to that in the South China Sea. The presence of ~500-kyr cycles over the last 5 Myr is demonstrated by wavelet analysis of the $\delta^{13}C$ record from ODP Site 846, equatorial Eastern Pacific (Figure 4b).

[16] The South Atlantic is represented by ODP Site 1090 just north of the modern Antarctic Polar Front [*Gersonde and Hodell*, 2002]. The $\delta^{13}C$ maxima are visible in both the planktonic and benthic records (Figures 7j and 7k) [*Venz and Hodell*, 2002], and the 500-kyr-long cycles are also displayed in all the carbonate percent, opal percent, lithogenic percent and organic carbon percent curves [*Diekmann and Kuhn*, 2002]. The planktonic $\delta^{13}C$ sequence at ODP Site 758 (Figure 7i) [*Chen et al.*, 1995] from the Bay of Bengal, Indian Ocean, resembles that at Site 1143 (Figure 2a), with even more prominent expression of the $\delta^{13}C$ maxima at Site 758, especially $\delta^{13}C$ max IV. The coarse fraction curve (Figure 7h) [*Bassinot et al.*, 1994a] mirrors that of $\delta^{13}C$ since $\delta^{13}C$ max IV. Spectral analysis shows that the long cycles exist over the 5 Myr $\delta^{13}C$ record at that site (Figure 3d).

[17] After the ocean by ocean comparison, it becomes clear that several long-period cycles of ~500 kyr are recognizable in all $\delta^{13}C$ records, and $\delta^{13}C$max-I to IV appear to be global events. A similar long-period signal is recognizable in lithological and geochemical records in the oceans. Figure 8 compares the Site 1143 benthic $\delta^{13}C$ record with curves of coarse fraction percent (>63 mm) at the same site, of a composite coarse-fraction index for the Indian Ocean [*Bassinot et al.*, 1994a], and the noncarbonate content of stacked subtropical South Atlantic cores, determined from magnetic susceptibility [*Schmieder et al.*, 2000] (Figures 8b, 8c, 8d, and 8h). Grey bars denote $\delta^{13}C$max-I to IV. All show similar 500 kyr cycles. At shorter wavelengths the relationships between the curves are not the same; even so, the coherence between several cores is high at the

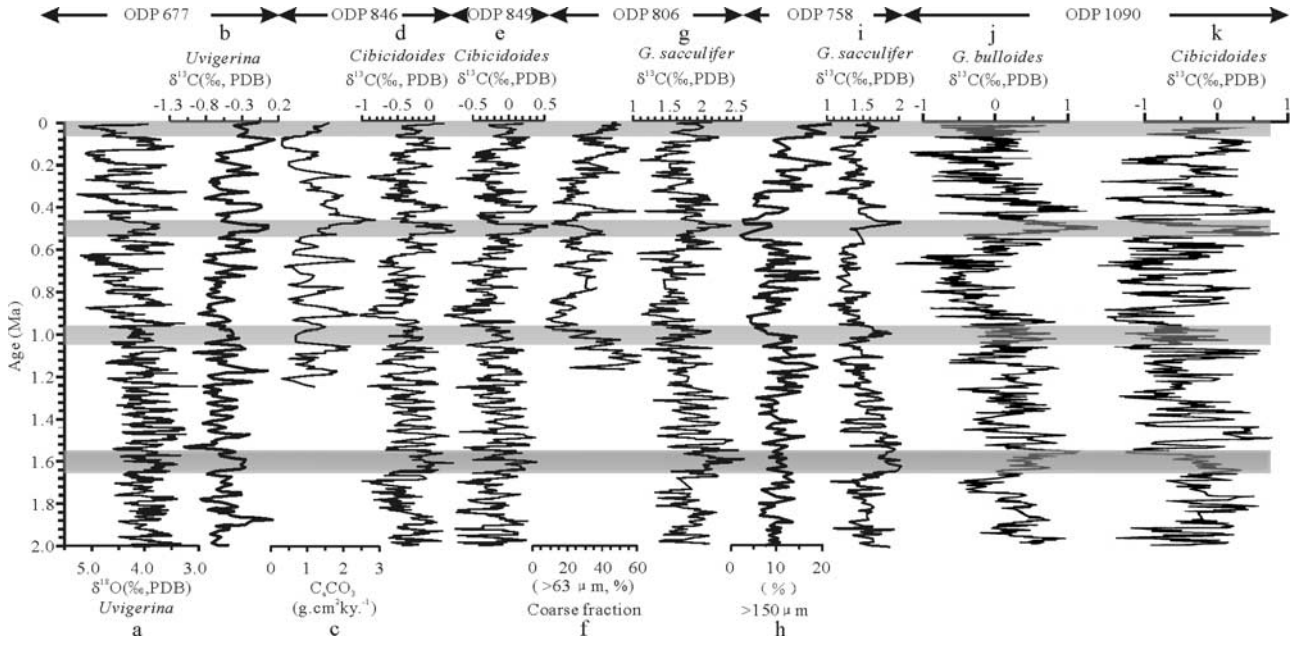

Figure 7. Carbon isotope and carbonate records over the last 2 Myr in various oceans. eastern Pacific, ODP Site 677: (a) $\delta^{18}O$ of benthic foraminifers [*Shackleton et al.*, 1990] and (b) $\delta^{13}C$ of benthic foraminifers (*Raymo et al.* [1990], modified to fit the age model in Figure 7a). ODP Site 846: (c) carbonate accumulation rate (mg/cm^2/kyr) [*Emeis et al.*, 1995] and (d) $\delta^{13}C$ of benthic foraminifers [*Shackleton et al.*, 1995]. ODP Site 849: (e) $\delta^{13}C$ of benthic foraminifers [*Mix et al.*, 1995]. Western Pacific, ODP Site 806: (f) coarse fraction (>63 μm) (data from *Yasuda et al.* [1993]) and (g) $\delta^{13}C$ of planktonic foraminifers [*Schmidt et al.*, 1993]. Indian Ocean, ODP Site 758: (h) coarse fraction percent (>150 μm) [*Bassinot et al.*, 1994a] and (i) $\delta^{13}C$ of planktonic foraminifers [*Chen et al.*, 1995]. South Atlantic, ODP Site 1090: (j) $\delta^{13}C$ of planktonic foraminifers and (k) $\delta^{13}C$ of benthic foraminifers [*Venz and Hodell*, 2002].

Milankovitch periods (e.g., Site 1143 *Cibicidoides* $\delta^{13}C$, and the South Atlantic magnetic susceptibility stack). There are many factors determining lithology of a given site, but the long-term cycles under discussion are one of the major features. The carbonate records, as seen from Figures 6–7, are complex and vary greatly between regions and locations. The $\delta^{13}C$ maxima, for example, correspond to carbonate dissolution in the Indo-Pacific, but enhanced preservation in the Atlantic. Nevertheless, the 500-kyr cycles are common to all carbonate curves, and also to other records such as the nitrogen isotope $\delta^{15}N$ of bulk sediments at ODP Site 722, Arabian Sea (Figure 8i) [*Altabet et al.*, 1999], and ice rafted debris (IRD)% at Site 982, near the Arctic (Figure 8j) [*Venz and Hodell*, 1999], at least for the last million years. The 500-kyr cycle is best displayed between $\delta^{13}C$ max-II and III, as seen from opal percent, lithogenic percent and organic carbon percent curves at ODP Site 1090 from the Southern Ocean (Figures 8e–8g) [*Diekmann and Kuhn*, 2002].

5. Details of $\delta^{13}C$ Maximum Episodes

[18] We now draw attention to shorter-term changes that occurred at widely separated sites around the times of major $\delta^{13}C$ maxima. At first we focus on the episode centered on $\delta^{13}C$max-II (Figure 9), which shows significant features that appear elsewhere in the record. Following the peak in MIS 13, there is a large (~1‰) fall in $\delta^{13}C$ of benthic *Cicidoides* spp in MIS 12, followed in turn by a sharp rise into MIS 11 (Figures 5a and 9b) [*Wang et al.*, 2003]. The MIS 12–11 transition not only is sharply defined by carbon isotopes but also shows the largest oxygen isotope shift (~2.5‰) at Site 1143. In fact, the MIS 12–11 transition is the largest change of $\delta^{18}O$ globally in the last 6 Myr [*Droxler and Farrell*, 2000], and is a key episode in the global climate system that cannot be explained by the minor amplitude in the orbitally induced insolation changes (the stage 11 problem; *Imbrie et al.* [1993]).

[19] The isotopic turnover at $\delta^{13}C$max II is accompanied by changes of upper ocean structure as indicated by changing abundances of nannoplankton that live at different depths. At Site 1143, the lower thermocline-dwelling nannoplankton *F. profunda* shows peak abundance at $\delta^{13}C$max-II and then decreases rapidly (Figures 5g and 9d). At the same time, the small mixed layer nannoplankton *Gephyrocapsa* increases sharply, both in the South China Sea (as noted above), and in cores from the tropical Pacific and tropical Atlantic (Figure 9h) [*Bollman et al.*, 1998]. The switch from *F. profunda* to small *Gephyrocapsa* at these widely separated sites indicates a widespread switch in upwelling and nutrient supply, because the relative abundance of *F. profunda* increases with reduced upwelling and reduced nutrient supply, which leads to low mixed layer productivity [*Molfino and McIntyre*, 1990]. In contrast, small

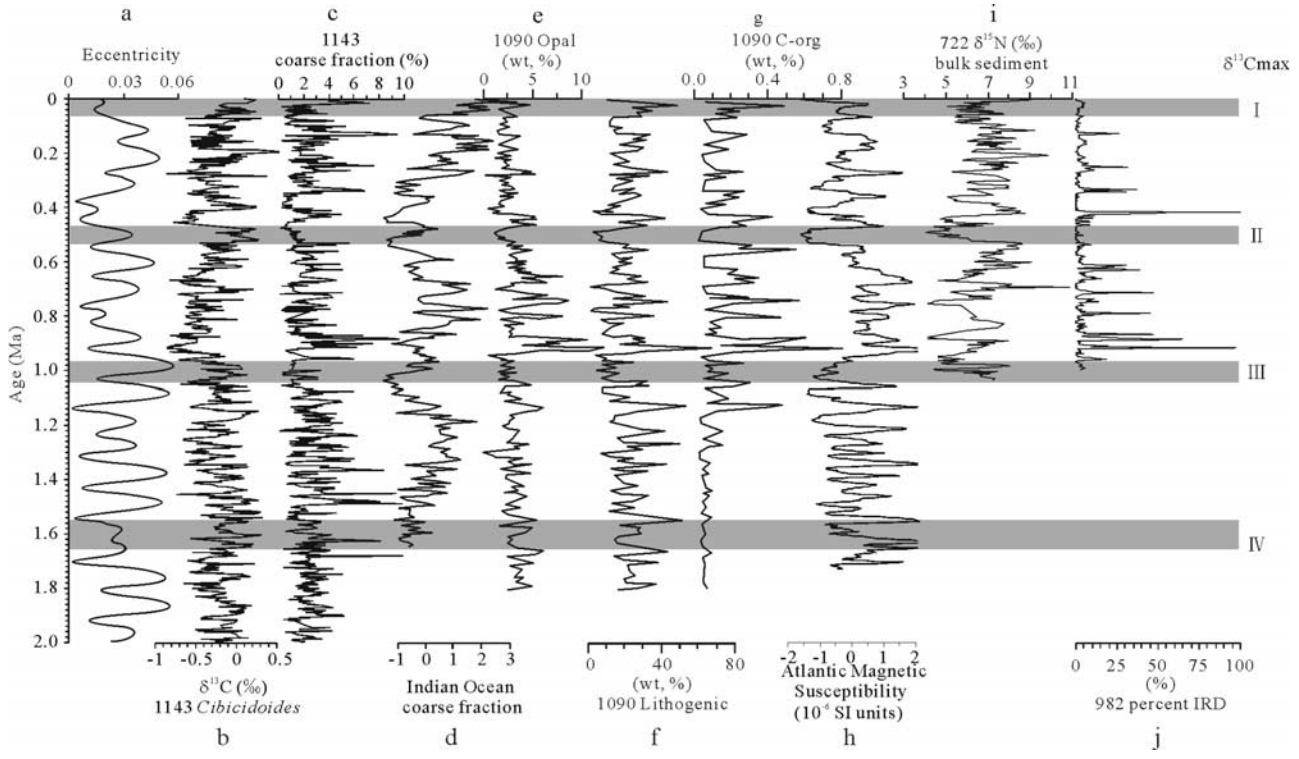

Figure 8. Comparison of $\delta^{13}C$ with lithological and geochemical variations over the last 2 Myr. (a) Eccentricity variation in orbital forcing [*Laskar*, 1990]. Western Pacific, ODP Site 1143: (b) benthic $\delta^{13}C$ and (c) coarse fraction (>63 μm) percent. Indian Ocean: (d) composite coarse fraction index, tropical Indian Ocean [*Bassinot et al.*, 1994a]. South Atlantic, ODP Site 1090: (e) opal percent, (f) lithogenic percent, and (g) organic carbon percent [*Diekmann and Kuhn*, 2002]. (h) Subtropical South Atlantic magnetic susceptibility stack (SUSAS) which is negatively related to $CaCO_3$ percent [*Schmieder et al.*, 2000]. Equatorial Indian, ODP Site722: (i) bulk sediment $\delta^{15}N$ (*Altabet et al.* [1999]; curve modified to fit the age model in the work of *Clemens et al.* [1996]). North Atlantic, ODP Site 982: (j) ice-rafted debris (IRD) [*Venz and Hodell*, 1999].

Gephyrocapsa increases with upwelling and indicates increased mixed layer productivity [*Gartner*, 1988]. This is supported by the abrupt increase of *G. bulloides* percent in planktonic foraminiferal assemblage from MIS 13 to 12 at Site 1143 (Figure 5e).

[20] There is evidence that $\delta^{13}C$max-II and the transition from MIS 13 to MIS 12 was not only marked by widespread increase of nutrient supply, upwelling and mixed layer nannoplankton production, but also by major climatic events. In the equatorial Indian Ocean, an exceptional $\delta^{18}O$ depletion peak at 0.525 Ma in Core MD 900963 was interpreted by *Bassinot et al.* [1994b] as a large freshwater discharge to the ocean (event Y; Figure 9f). This coincides with a thick sapropel layer in the eastern Mediterranean that indicates high rainfall (Sap A: Figure 9e) [*Rossignol-Strick et al.*, 1998]. Oxygen isotopes suggest that high rain/high freshwater discharge at these sites was interrupted around 0.51 Ma and then resumed. Unusually high precipitation in the Amazon Basin in MIS 13 is suggested by extraordinarily high terrigenous flux in ODP holes at Ceara Rise (Figure 9g) [*Harris et al.*, 1997], while a period of exceptional warmth and humidity is indicated on the Chinese Loess Plateau, where paleosol S5-1 is distinguished by the highest values of magnetic susceptibility and deepest weathering [*Guo et al.*, 1998] (Figure 9l). The increased humidity at the beginning of MIS 13 also led the minimal eolian dust transported from the Asian continent to the Pacific Ocean as recorded at KK75-02 (38°37′N, 179°20′E; Figure 9k) [*Janecek and Rea*, 1984]. Finally, at ~30°S in the southern Atlantic, thick laminated, near-monospecific diatom ooze layers at the beginning of MIS 13 imply reduced ventilation of the water column replaced by carbonate deposits immediately afterward (Figures 9i and 9j) [*Schmieder et al.*, 2000; *Gingele and Schmieder*, 2001]. Arguably, the diatom ooze reflects silica pulses derived from high river discharges, with enhanced chemical weathering in their catchments, or from incursions of silicate-enriched water of higher latitudes.

[21] Similar events to those described from MIS 13 to 11 might have taken place at other $\delta^{13}C$max, but available data diminish with increasing age. Figure 10 shows a number of events around the $\delta^{13}C$max III (MIS 27–29, 0.97–1.04 Ma), partly during the later part of Jaramillo event. MIS 31 at the base of the Jaramillo (1.07 Ma) was distinguished by the highest summer insolation of the last 5 Myr, and the unusual warming caused partial or complete retreat of the West

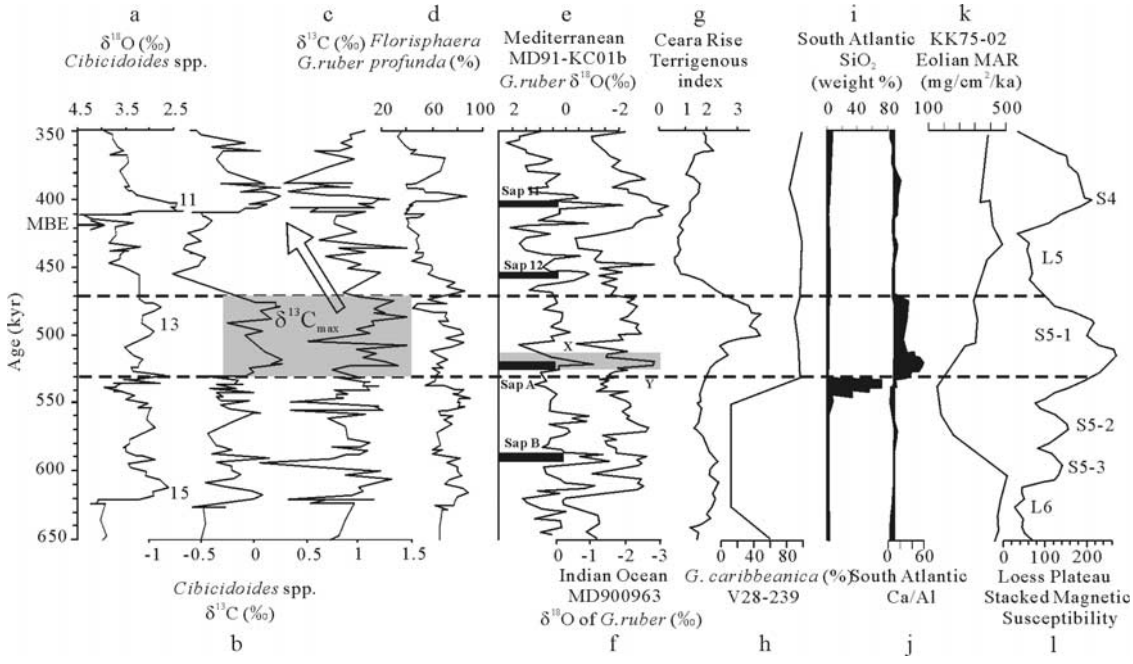

Figure 9. Records of events around the δ^{13}Cmax-II in MIS 13 (between dashed lines). ODP Site 1143, South China Sea: (a) benthic δ^{18}O (Mid-Brunhes Event (MBE)), (b) benthic δ^{13}C, (c) plankton δ^{13}C, and (d) *Florisphaera profunda* percent. Other oceans: (e) δ^{18}O record of *G. ruber* with sapropel layers (Sap) in core KC01b, Ionian Sea, Mediterranean (36°15′N, 17°44′E, water depth 3643 m). "Sap A" is abnormal. [*Rossignol-Strick et al.*, 1998] (f) δ^{18}O record of *G. ruber* in core MD 900963, equatorial Indian Ocean (5°03′N, 73°52′E, water depth 2446 m) showing δ^{18}O events Y and X [*Bassinot et al.*,1994b]. (g) "Terrigenous index" (relative terrigenous mass accumulation rate) at ODP Sites 929/925, Ceara Rise, equatorial Atlantic [*Harris et al.*, 1997]. (h) Small *Gephyrocapsa* percent (*G. caribbeanica*) in coccolith flora excluding *F. profunda* percent, V28−239, tropical Western Pacific (3°15′N, 159°11′E, water depth 3490 m) (a schematic curve based on the original depth-plotted curve from *Bollmann et al.* [1998]). (i) Biogenic opal percent and (j) Ca/Al ratio indicating carbonate preservation in core GeoB 3813-3 [*Gingele and Schmieder*, 2001]. (k) Eolian mass accumulation rate in core KK75-02, northern Pacific (38°37′N, 179°20′E) [*Janecek and Rea*, 1984]. (l) Stacked magnetic susceptibility from Loess Plateau, China (S,-paleosol, L, loess) [*Guo et al.*, 1998].

Antarctic Ice Sheet [*Scherer et al.*, 2003]. This was followed by a relatively prolonged period of low-frequency oscillations within the Jaramillo until MIS 28 [*Kucera and Kennett*, 2002] (see Figure 10a), suggesting a relative stability of the ice sheets. However, there were significant changes in the low latitudes within this time interval. Immediately after the MIS 31 warming, equatorial Africa experienced a remarkable cooling at MIS 30 (1.05 Ma), as witnessed by an abrupt increase of *Podocarpus* percent in pollen assemblages from ODP Site 1075, Congo Fan (Figure 10i). This same event has been reported from South America, where the upper Andean forest line dropped for the first time in more than 400 kyr, indicating the MIS 30 climate cooling both in tropical Africa and South America [*Dupont et al.*, 2001].

[22] The tropical climate changes described above were a prelude to δ^{13}Cmax-III in the ocean, which began during MIS 29 at 1.04 Ma, in the middle of the Jaramillo (Figures 10b and 10c). As seen from the records at Site 1143 (Figure 10b), the benthic δ^{13}C negatively shifted by about 1‰ approaching MIS 23, leading to a major ice sheet expansion at the MIS 23/22 turn (Figure 10a), a sequence resembling that of δ^{13}C max II (Figures 9a–9c). A high-resolution study at Ceara Rise, tropical Atlantic (Figure 10e), confirms the association of δ^{13}Cmax-III with sudden changes in the patterns of glacial cycles, from small-amplitude variations in MIS 28 and 26 to very large ones in MIS 22 [*Bassinot et al.*, 1997; *Bickert et al.*, 1997]. The δ^{13}Cmax-III event, like δ^{13}Cmax-II, probably was a period of enhanced precipitation in the tropics as shown by the sudden decline of *Spiniferites* in dinoflagellate assemblages following the δ^{13}Cmax-III (Figure 10j) at Site 1075, Congo Fan, which is interpreted as a reduction of the influence of the Congo freshwater plume and river-induced upwelling over the site [*Dupont et al.*, 2001].

[23] Similarly, the δ^{13}Cmax-III around 1.0 Ma is accompanied by a major change in $CaCO_3$% off the Amazon estuary (Figure 10g) [*Bassinot et al.*, 1997], in aragonite percentage at the Maldives [*Droxler et al.*, 1990] and in carbonate preservation in various oceans (Figure 8). The nannoplankton assemblages also suggest significant changes in upper ocean structure at the δ^{13}Cmax-III, when *F. profunda*

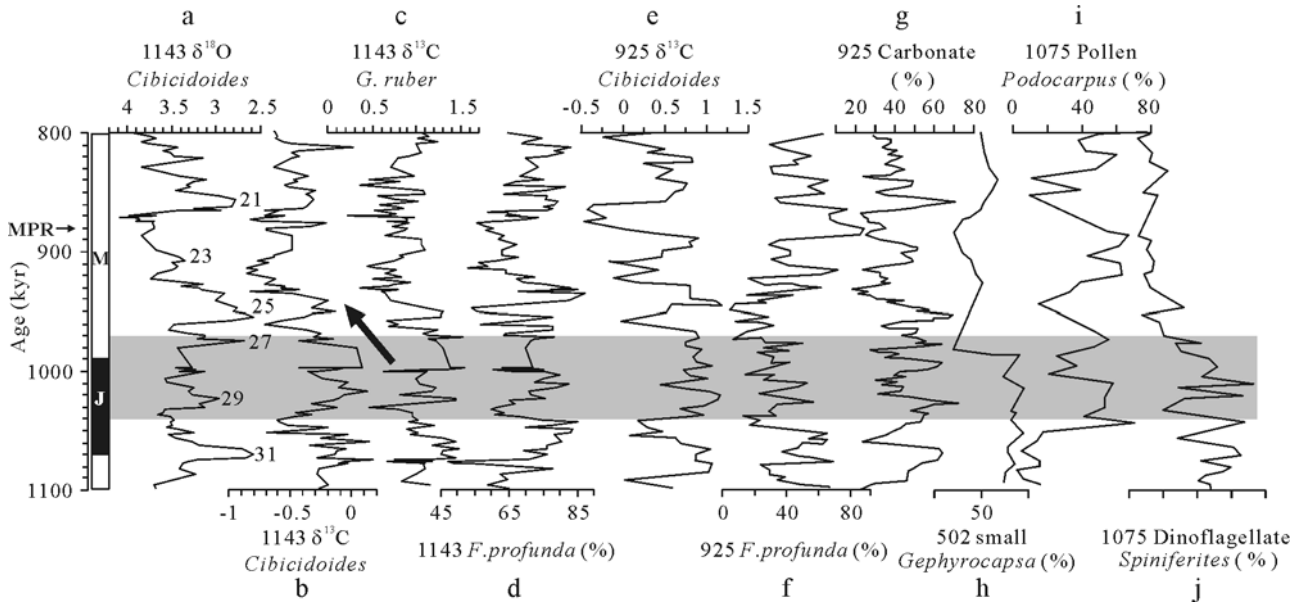

Figure 10. Records of events around the δ^{13}Cmax-III in MIS 27–29 (between dashed lines). Left column shows paleomagnetic age (M, Matuyama; J, Jaramillo). ODP Site 1143, South China Sea: (a) benthic δ^{18}O (Mid-Pleistocene Revolution (MPR)), (b) benthic δ^{13}C, (c) plankton δ^{13}C, and (d) *Florisphaera profunda* percent. ODP Site 925, equatorial Atlantic: (e) benthic δ^{13}C record at Site 925 [*Bickert et al.*, 1997], (f) *Florisphaera profunda* percent, and (g) carbonate percent [*Bassinot et al.*, 1997]. ODP Site 1075, southern Atlantic (4°47′N, 10°04′E, water depth 2996 m): (h) pollen *Podocarpus* percent and (i) dinoflagellates *Spiniferites* percent [*Dupont et al.*, 2001]. DSDP Site 502 (11°29′N, 79°23′E, water depth 3051 m), Caribbean Sea: (j) small *Gephyrocapsa* percent (*Gartner* [1988] age model based on oxygen isotope data from *Prell* [1982]).

percent reached its maximum at Site 1143 (Figures 5g and 10d) but minimum at Site 925 (Figure 10f) [*Bassinot et al.*, 1997]. Despite the opposing changes in the two oceans, the δ^{13}Cmax-III represents a turning point in near-surface water conditions, and this can also be seen from the planktonic and radiolarian assemblages at Site 1143 (Figures 5e, 5f, and 5i), as well as in carbonate accumulation and nannoplankton composition.

[24] δ^{13}Cmax-IV (MIS 53–57, 1.55–1.65 Ma) is characterized by the isotope and carbonate changes shown in Figures 5–7. Although the limited data available preclude any possibility for a detailed view of the event itself, the climate consequences of δ^{13}Cmax-IV are emerging in the literature. For example, Africa aridity increased and obliquity-forced climate variability increased at 1.6 Ma [*DeMenocal*, 1995]. In the Southern Ocean, MIS 52 (1.55 Ma) marked a new step in the development of glacial climate, comparable to MIS 22, the Mid-Pleistocene Transition. At ODP Site 1090 the benthic δ^{13}C drastically increased its range of fluctuations during MIS 52 (Figure 7k), then the δ^{18}O variability increased from 0.5‰ to 1‰ in the plankton record afterward and remained within this range until ~0.9 Ma [*Venz and Hodell*, 2002, Figure 6]. MIS 52 was the beginning of the late Pleistocene pattern whereby glacial δ^{13}C values in the Southern Ocean are less than those in the Pacific, implying the expansion of sea ice cover in the southern Ocean. Since then, heat transport from low to high latitudes began to strengthen according to the propagation of tropical semiprecessional cycles to higher latitudes [*Rutherford and D'Hondt*, 2000]. Therefore δ^{13}Cmax IV led to enhancement of glacial climate like its successors.

6. The 500-kyr Cycle, Orbital Forcing, and Climate

[25] The idea that marine core records show long-term cycles superimposed on glacial cycles is not new. *Briskin and Berggren* [1975] detected 500 kyr periodicity in a foraminifera-based winter temperature record from tropical North Atlantic core V16-205, and a similar periodicity has since been identified in tropical carbonate records [*Droxler et al.*, 1990; *Bassinot et al.*, 1994a]. Others have recognized long cycles in Quaternary δ^{13}C records [*Keigwin and Boyle*, 1985; *Raymo et al.*, 1990; *Bickert et al.*, 1993; *Mix et al.*, 1995]. Some authors sought to explain these long cycles in terms of the amplitude of the 21-kyr precessional cycle, which is modulated by eccentricity and varies with periods of 90–100 kyr and 413 kyr [e.g., *Briskin and Harrell*, 1980]. However, the 500 kyr cycle found in high-resolution records, reviewed above, is significantly longer than 413 kyr and, as Figure 8 shows, the timing of δ^{13}Cmax-II and δ^{13}Cmax-III are substantially offset from the nearest periods when the amplitude of the eccentricity cycle was low (~350–450 kyr and ~750–850 kyr).

[26] We note that this appears to be a Quaternary pattern: before the Quaternary, the 413-kyr cycle of eccentricity affected low-latitude climate and is found, for example, in

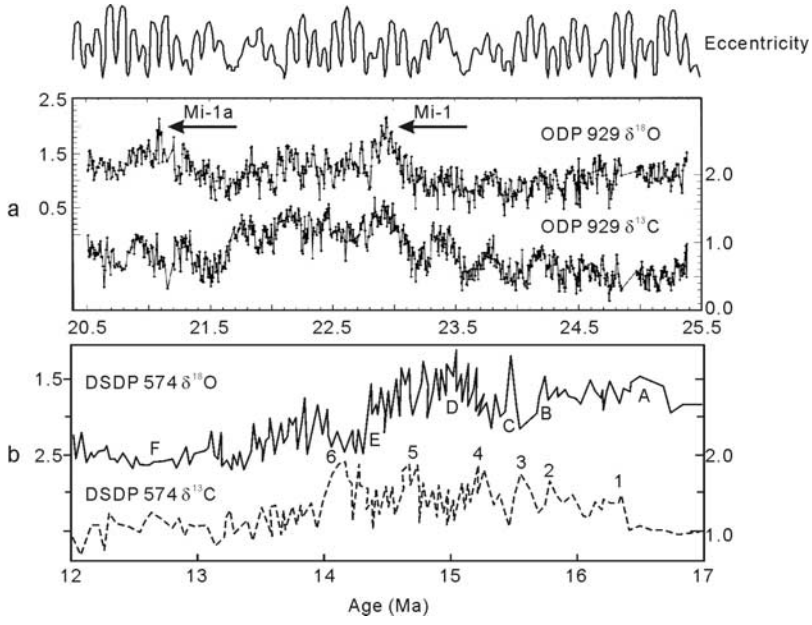

Figure 11. Comparison of deep-sea benthic $\delta^{18}O$ and $\delta^{13}C$ records in the late Cenozoic: (a) late Oligocene-early Miocene, 20.5–25.4 Ma, ODP Site 929, western equatorial Atlantic (5°58′N, 43°44′W, water depth 4358 m), compared with orbital eccentricity [*Paul et al.*, 2000]. (b) Middle Miocene, 12–17 Ma, DSDP Site 574, eastern equatorial Pacific (4°12′N, 133°19′W, water depth 4561 m). A–F denote $\delta^{18}O$ events, and 1–6 denote $\delta^{13}C$ maximum events CM1–CM6 [*Woodruff and Savin*, 1991]. Note that the $\delta^{18}O$ curves in Figures 11a and 11b are shown in opposite directions.

Plio-Pleistocene monsoon records in the Mediterranean [*Wehausen and Brumsack*, 1999] and off western Africa [*Tiedemann et al.*, 1994]. It is also found in late Oligocene-early Miocene oceanic isotopes and carbonates [*Zachos et al.*, 2001]. Figure 11 shows $\delta^{18}O$ and $\delta^{13}C$ records of the middle Miocene at DSDP Site 574, eastern equatorial Pacific, and of the late Oligocene-early Miocene at ODP site 929, western equatorial Atlantic; in both cases the long-term variations in $\delta^{13}C$ and $\delta^{18}O$ display the same ~413-kyr cycles [*Woodruff and Savin*, 1991; *Paul et al.*, 2000]. Prior to the formation of ice sheets in the Northern Hemisphere, therefore, $\delta^{13}C$ covaried with $\delta^{18}O$ in the ocean records, but in Quaternary times the 413-kyr cyclicity waned in the $\delta^{18}O$ records and apparently "stretched" into 500 kyr in $\delta^{13}C$. The change will be discussed elsewhere; here we are concerned only with showing that the 500 kyr cycle is clearly revealed in the Quaternary by $\delta^{13}C$ but not by $\delta^{18}O$.

[27] While $\delta^{18}O$ is a proxy for global ice volume, $\delta^{13}C$ records carry signals of changes in the global carbon system, and respond to changes in both oceanic and terrestrial processes both at higher and lower latitudes. The strong high-frequency $\delta^{13}C$ variability seen in Figures 6–7 at least partly reflect glacial-interglacial changes of global biomass (reviewed by *Crowley* [1995]). The glacial-interglacial amplitudes of benthic $\delta^{13}C$ changes are larger in the Atlantic than elsewhere and reflect the changing intensity of North Atlantic Deep Water (NADW), which varies with growth and decay of the northern ice sheets [*Raymo et al.*, 1990; *Bickert et al.*, 1997]. An example is the remarkable negative excursion at MIS 12 in benthic $\delta^{13}C$ curves at all sites in Figures 6–7 but Site 982 (water depth 1134 m, Figure 6b) which is washed by intermediate instead of deep waters [*Venz and Hodell*, 2002]. However, we infer that the long-term cycles in $\delta^{13}C$ have a tropical origin because of their presence in carbonate and tropical phytoplankton records. The effects of linked terrestrial and climatic processes also occur at different scales, and are illustrated by the complex association of high rates of weathering and of terrigenous inputs at the time of $\delta^{13}C$max-II, described above.

[28] Although *Keigwin and Boyle* [1985] suggested that longer-term $\delta^{13}C$ cycles reflect the effect of precession-cycle amplitude on climate and thus on biomass, *Crowley* [1995] recognized that the matter is more complex. The 500 kyr cycles may reflect secular changes in "rain ratio," which is the organic versus inorganic ratio in oceanic carbon deposition [*Archer et al.*, 2000] and is basically the ratio of diatoms to coccoliths. Diatom blooms in the ocean, particularly those of "giant diatoms," may result in a remarkably increased organic/inorganic ratio in carbon deposition. A $\delta^{13}C$ maximum occurs when the ratio is unusually high. This is confirmed by the Pliocene opal record from the Subarctic northwest Pacific. The record of opal mass accumulation rate between 5.3 and 2.73 Ma from the Subarctic northwestern Pacific shows a remarkable correlation with the benthic $\delta^{13}C$ curve from the Caribbean Sea [*Haug et al.*, 1999], both displaying ~400-kyr cycles. A significant correlation was also found between the opal record in the South Atlantic Ocean and benthic $\delta^{13}C$ of the last 2 Myr, with a similar long-term cyclicity [*Berger et al.*, 2002], implying a link between diatom sedimentation and global ocean nutrient chemistry.

[29] On this basis we propose that variations in total diatom sedimentation in the global ocean account for the

quasiperiodic occurrences of δ^{13}Cmax. In the Cenozoic the global ocean has many times experienced migration of siliceous deposition zones, involving fractionation between ocean basins [*Barron and Baldauf*, 1989] and between latitudes [*Berger et al.*, 2002]. Occurrences of diatom layers indicative of "giant diatom" blooms have been repeatedly reported from the open ocean [e.g., *Broecker et al.*, 2000; *De Deckker and Gingele*, 2002]. As "giant diatoms" can use nutrients from the underlying nutricline, their blooms may occur in the open oligotrophic ocean where surface nutrient levels are minimal [*Villareal et al.*, 1999]. On a global basis diatom deposition can make a large contribution to carbon reservoir changes in the ocean. Mat-forming diatoms have been suggested to be the source of high organic carbon in Mediterranean sapropels and mid-Cretaceous black shales [*Kemp et al.*, 1999; *Sancetta*, 1999]. However, their role in Cenozoic paleoclimate studies has been underestimated because of their patchy distribution in space and time [*Shipe et al.*, 1999] and poor preservation of biogenic opal in the ocean [*Sancetta et al.*, 1991].

[30] Presumably, the quasiperiodic occurrence of δ^{13}C maxima is associated with two processes in Si cycling: the silica supply by rivers, which is dependent on weathering rate, and the incursion of silica-enriched waters which directly triggers the "giant diatom" blooms. The former process is known to display long-term cycles. The diatom/coccolith ratio tends to increase with the availability of silica for biological uptake in the ocean, which predominantly comes from tropical rivers [*Tréguer et al.*, 1995]. Evidence that weathering and river discharge were unusually high during δ^{13}Cmax-II was reviewed earlier and includes sapropel formation in the eastern Mediterranean and strong pedogenesis on the Chinese loess plateau (see Figure 9), as well as evidence for extraordinarily high terrigenous flux at Ceara Rise [*Harris et al.*, 1997]. Actually, the effect of long-term cycles in weathering intensity on oceanic δ^{13}C was proposed much earlier. For example, the reduced amplitude in the δ^{13}C signal during MIS 2 relative to MIS 4 and 6 was attributed to the reduction of precessional forcing within the eccentricity cycle [*Keigwin and Boyle*, 1985; *Crowley*, 1995].

[31] The incursion of silica-enriched water probably involves tropical-extratropical interactions, but the nature of its long-term quasiperiodicity requires further studies. Nonetheless, the link between diatom deposition and δ^{13}Cmax events is supported by records. As noted above, thick laminated diatom ooze layers occur at ~30°S in the southern Atlantic at the beginning of MIS 13 (Figure 9i) [*Schmieder et al.*, 2000; *Gingele and Schmieder*, 2001]. The intruded nutrient-rich deeper water not only triggers "giant diatom" bloom, but also affect other phytoplankton. Indeed, the deeper-dwelling nannoplankton *F. profunda* percent reached its maximum around δ^{13}Cmax-II and III at Site 1143 (Figure 5g), indicating that coccolith productivity in the mixed layer was low.

[32] To summarize, while the cause of the long-term cycles is unclear, the decrease following a δ^{13}C maximum appears to involve major reorganization of the global carbon and climate systems. Evidence cited above indicates that low-latitude climates during δ^{13}Cmax-II (MIS 13) were unusually wet, and that enhanced weathering and runoff supplied a high silica flux to the oceans, which in turn led to high diatom/coccolith ratios in the plankton and a high rate of organic carbon burial in marine sediments. Conditions switched rather rapidly in the transition to MIS 12: although the assembled isotopic records indicate that the next 500 kyr cycle passed through a broad trough around 200–300 kyr ago, the cycle began with a rapid descent from the δ^{13}C maximum to an early minimum accompanied by major glaciation in MIS 12 (Figure 9). The scenario at earlier δ^{13}C maxima might be somewhat different, but in terms of δ^{13}C and carbonate sedimentation patterns, δ^{13}Cmax-III and IV appear to have been similar, and δ^{13}Cmax-III was also associated with changes in upper ocean structure in the tropical ocean (Figures 5, 8, and 10).

7. Discussion: Major Stages of the Quaternary and Global Carbon Shifts

[33] It is widely considered that Quaternary glacial cycles have passed through two changes of regime. *Berger et al.* [1994] placed the first at 0.9 Ma (MIS 22), when the boreal ice sheets increased in size and the prevailing glacial cyclicity changed from ~40 kyr to ~100 kyr, and referred to it as the "Mid-Pleistocene Revolution" (MPR). *Raymo et al.* [1997] use the term "Mid-Pleistocene Transition" or MPT for the same event. The second, known as the Mid-Brunhes Event (MBE) [*Jansen et al.*, 1986], occurred at the termination of MIS 12 (~0.4 Ma) and is marked by the largest amplitude shift of δ^{18}O of the last 6 Myr [*Droxler and Farrell*, 2000].

[34] Notably, both the MPR and MBE were preceded by δ^{13}Cmax events: δ^{13}Cmax-II before the MBE and δ^{13}Cmax-III before the MPR. This seems to us to be highly significant and suggests that changes within the carbon system can modify the response of the ice climate system to orbital forcing, and that episodes of substantial reorganization of the carbon system may be involved. The long-term cycles in weathering intensity in tropical areas may give rise to increased flux of Si from land to ocean, which may change the phytoplankton composition and hence the organic/inorganic carbon ratio in sediments. More work is needed to find out the mechanism behind the observed changes in carbon cycling.

[35] Although we cannot yet resolve the question of mechanism, δ^{13}Cmax-II and δ^{13}Cmax-III emerge as key events that divide the Quaternary into three parts (Figure 12). Various subdivisions of the Quaternary have previously been proposed. For example, *Berger et al.* [1994], while emphasizing the significance of the MPR in the δ^{18}O record at ODP Site 806 (Ontong-Java Plateau), proposed a triple division of the last 2 Myr based on dominant periods in glacial cycles; they named the three divisions as the "Milankovitch," "Croll" and "Laplace" chrons, each of 15 obliquity cycles or 600 kyr in duration (Figure 12c). This scheme depicts the progressive change in glacial cyclicity but the age boundaries are rather arbitrary and, while others have retained three divisions, they have placed the boundaries differently. From magnetic susceptibility logs of subtropical South Atlantic cores, *Schmieder et al.* [2000] concluded

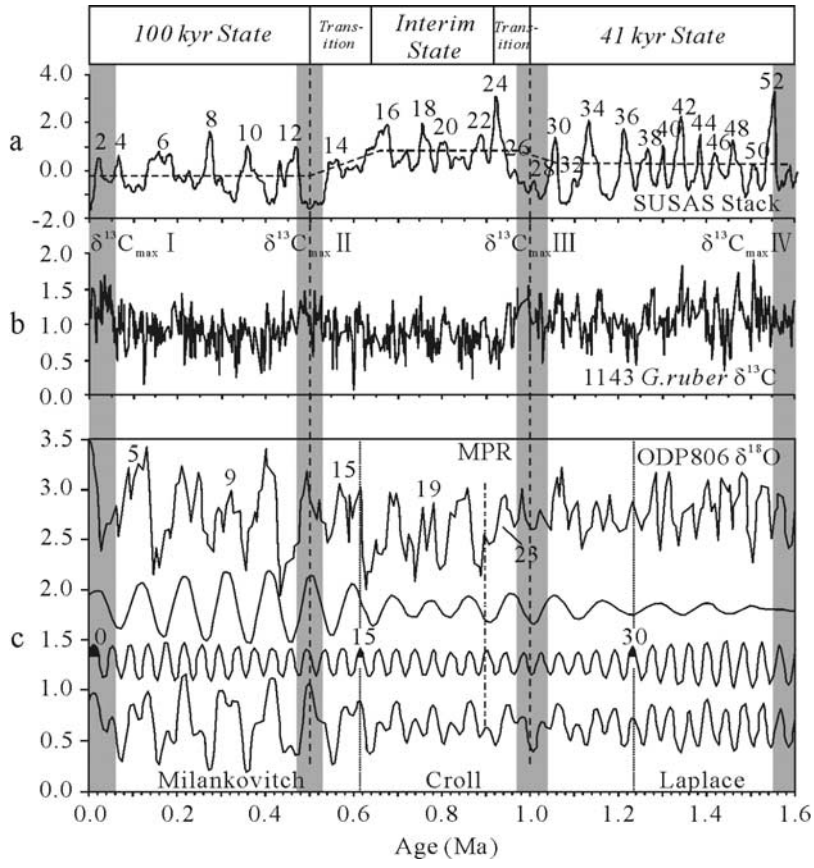

Figure 12. Subdivision of the last 1.6 Myr of the Quaternary into major climate stages. (a) Triple division into "100 kyr state," "interim state," and "41 kyr state" based on Subtropical South Atlantic Susceptibility (SUSAS) stack [*Schmieder et al.*, 2000]. (b) Triple division based on δ^{13}Cmax events, represented by planktonic δ^{13}C of ODP Site 1143. (c) Triple division into "Milankovitch," "Croll," and "Laplace" chrons based on predominant climate cyclicity represented by benthic δ^{18}O of ODP Site 806, Ontong Java Plateau, western tropical Pacific [*Berger et al.*, 1994].

that "the MPT (Mid-Pleistocene transition) should not be regarded as a gradual transition from a "41 kyr world" to a "100 kyr world," but rather as a third, contrasting state of the global circulation system," defined as "MPT interim state" between 0.5 Ma and 1.0 Ma (Figure 12a). These boundaries coincide exactly with δ^{13}Cmax-II and δ^{13}Cmax-III, identified in this paper, and reflect major steps in polar ice sheet development (Figure 12b). Prior to δ^{13}Cmax-III, the 41 kyr obliquity cycle was dominant; δ^{13}Cmax-III led to the MPR and onset of the 100-kyr world, and δ^{13}Cmax-II led to the MBE and initiated the maximal amplitude of 100-kyr glacial cycles. We note that system changes at the time of our earliest maximum, δ^{13}Cmax-IV, have not yet been identified, although it was suggested recently that the 100-kyr cyclicity in climate might have started at 1.5 Ma [*Rutherford and Hondt*, 2000], and that sea-ice expansion and a fundamental change in South Ocean deep water circulation took place after MIS 52, at about 1.55 Ma [*Venz and Hodell*, 2002].

[36] The triple division of the Quaternary is based on carbon reservoir changes in the ocean, as we discussed, but it is ubiquitous in all Quaternary sequences with sufficient length and resolution. The 500-kyr cycles can be seen from the monsoon upwelling recorded in δ^{15}N of bulk samples from Site 722, Arabian Sea (Figure 8i) [*Altabet et al.*, 1999] to ice rafted debris (IRD)% at Site 982, near the Arctic (Figure 8j) [*Venz and Hodell*, 1999]. Even microfossil evolution in Quaternary is associated with the δ^{13}Cmax events as illustrated by the variations of maximal size of a planktonic foraminifer *Neogloboquadrina pachyderma* at Site 982 [*Kucera and Kennett*, 2002].

[37] Paleorecords are significant because they provide scientific background for prediction of the future. However, opinions in the scientific community are mixed in terms of the timing of the next glaciation, and the divergence in views is rooted in different estimations of the natural trend in carbon cycling change: Some scientists assume the declining late Cenozoic CO_2 level will continue and believe a new glaciation is coming [*Raymo*,1997]; but others consider that CO_2 variations in the next 130-kyr may only repeat what occurred in the past 130-kyr and conclude that a new glaciation will start 50-kyr from now [*Berger and Loutre*, 2002]. Neither of these two views has taken into account the periodicity in carbon cycling itself, and the presumed CO_2 trends are groundless in both cases. Noticeably, the Earth is now again passing through a new carbon

event, δ^{13}Cmax-I, which started some 50–60 kyr ago in MIS 3 or 4. There are signs of unusually warm and humid conditions in middle MIS 3 in Eastern Asia, including abnormally high lake levels and high magnetic susceptibility in the loess-paleosol sequence [*Shi et al.*, 1999] and abnormal depletion of planktonic δ^{18}O in the Sulu Sea [*Linsley*, 1996]. What will this event lead to: an unprecedented expansion of the ice sheet? It is crucial that we understand the physical and climatic meaning of the long-term carbon cycle if we are to predict the future trend of natural changes of the global climate.

8. Conclusions

[38] 1. Analyses of the deep-sea sediment sequence recovered from ODP Site 1143, southern South China Sea, and comparisons with long sequences from over the global ocean reveal a series of ~500 kyr cycles in δ^{13}C records. These "supercycles" also appear in carbonate preservation records, and the δ^{13}C maxima are inferred to reflect episodes when the carbon reservoirs and the upper ocean structure in the global ocean experienced profound reorganization, probably induced by changes in phytoplankton and the oceanic "rain ratio," associated with "giant diatom" blooms in the open ocean.

[39] 2. Four δ^{13}Cmax events took place within the Quaternary: δ^{13}Cmax-I, which began around 50–60 kyr in MIS 3 or 4; δ^{13}Cmax-II in MIS 13, 0.47–0.53 Ma; δ^{13}Cmax-III from MIS 27 to 29, 0.97 to 1.04 Ma; δ^{13}Cmax-IV from MIS 53–57, 1.55 to 1.65 Ma. Shifts in carbon reservoirs at these times apparently affected global climate, and at least two δ^{13}Cmax events are linked to major changes in glacial cyclicity: δ^{13}Cmax-II led to the MBE and δ^{13}Cmax-III to the MPR. Although δ^{13}Cmax usually occurred at times of minimal eccentricity forcing before the Quaternary, δ^{13}Cmax-II and δ^{13}Cmax-III are out of phase with this astronomical cycle and their origin remains an open question.

[40] 3. The three major stages of the Pleistocene subdivided by δ^{13}Cmax events represent successive steps of ice cap development. However, the long-term changes in carbon reservoirs on the Earth have their own periodicity and their own history, and do not simply follow ice cap variations in the Northern Hemisphere. Now the Earth system is again passing through a new carbon event, δ^{13}Cmax-I. Prediction of the future natural changes of the global climate is compromised without understanding the physical and climatic meaning of the long-term carbon cycles.

[41] **Acknowledgments.** The authors express their gratitude to John Chappell for significant improvement of our manuscript. James Kennett, Wolfgang Berger and Michael Sarnthein are greatly thanked for their encouraging discussions and constructive comments. We also thank two anonymous reviewers for their constructive comments, which helped to improve the manuscript. R. Tiedemann is acknowledged for providing carbon isotope data from ODP Site 659 and HUANG Wei for participation in figure preparation. In particular we thank the late Luejiang Wang and his wife for sampling the Site 1143 cores. This research used samples and data provided by the Ocean Drilling Program. ODP is sponsored by the U.S. National Science Foundation and participating countries under management of Joint Oceanographic Institutions, Inc. This work was supported by the NKBRSF (grant G2000078500) and the NNSFC (grant 4999560).

References

Altabet, M. A., D. W. Murray, and W. L. Prell (1999), Climatically linked oscillations in Arabian Sea denitrification over the past 1 m.y.: Implications for the modern N cycle, *Paleoceanography*, *14*, 732–743.

Archer, D., A. Winguth, D. Lea, and N. Mahowald (2000), What caused the glacial/interglacial atmospheric pCO_2 cycles?, *Rev. Geophys.*, *38*, 159–189.

Barron, J. A., and J. G. Baldauf (1989), Tertiary cooling steps and paleoproductivity as reflected by diatoms and biosiliceous sediments, in *Productivity of the Ocean: Present and Past*, edited by W. H. Berger, V. S. Smetacek, and G. Wefer, pp. 341–354, John Wiley, Hoboken, N. J.

Bassinot, F. C., L. Beaufort, E. Vincent, and L. D. Labeyrie (1994a), Coarse fraction fluctuations in pelagic carbonate sediments from the tropical Indian Ocean: A 1500–kyr record of carbonate dissolution, *Paleoceanography*, *9*, 579–600.

Bassinot, F. C., L. D. Labeyrie, E. Vincent, X. Quidelleur, N. J. Shackleton, and Y. Lancelot (1994b), The astronomical theory of climate and the age of the Brunhes-Matuyama magnetic reversal, *Earth Planet. Sci. Lett.*, *126*, 91–108.

Bassinot, F. C., L. Beaufort, E. Vincent, and L. Labeyrie (1997), Changes in the dynamics of western equatorial Atlantic surface currents and biogenic productivity at the "Mid-Pleistocene Revolution" (~930 ka), *Proc. Ocean Drill. Program Sci. Results*, *154*, 269–284.

Berger, A., and M. F. Loutre (2002), An exceptionally long interglacial ahead?, *Science*, *297*, 1287–1288.

Berger, W. H., M. Yasuda, T. Bickert, G. Wefer, and T. Takayama (1994), Quaternary time scale for the Ontong Java Plateau: Milankovitch template for Ocean Drilling Program Site 806, *Geology*, *22*, 463–467.

Berger, W. H., C. B. Lange, and M. E. Perez (2002), The early Matuyama diatom maximum off SW Africa: Aa conceptual model, *Mar. Geol.*, *180*, 105–116.

Bickert, T., W. H. Berger, S. Burke, H. Schmidt, and G. Wefer (1993), Late Quaternary stable isotope record of benthic foraminifers: Site 805 and 806, Ontong Java Plateau, *Proc. Ocean Drill. Program Sci. Results*, *130*, 411–420.

Bickert, T., W. B. Curry, and G. Wefer (1997), Late Pliocene to Holocene (2.6–0 Ma) western equatorial Atlantic deep-water circulation: Inferences from benthic stable isotopes, *Proc. Ocean Drill. Program Sci. Results*, *154*, 239–253.

Bollmann, J., K.-H. Baumann, and H. R. Thierstein (1998), Global dominance of *Gephyrocapsa* coccoliths in the late Pleistocene: Selective dissolution, evolution, or global environmental change?, *Paleoceanography*, *13*, 517–529.

Briskin, M., and W. A. Berggren (1975), Pleistocene stratigraphy and quantitative paleoceanography of tropical North Atlantic core V16-205, in *Late Neogene Epoch Boundaries*, edited by T. Saito and L. Burckle, pp. 167–198, Micropaleontol. Press, New York.

Briskin, M., and J. Harrell (1980), Time-series analysis of the Pleistocene deep-sea paleoclimatic record, *Mar. Geol.*, *36*, 1–22.

Broecker, W. S., E. Clark, J. Lynch-Stieglitz, W. Beck, L. D. Stott, I. Hajdas, and G. Bonani (2000), Late glacial diatom accumulation at 9°S in the Indian Ocean, *Paleoceanography*, *15*, 348–352.

Chen, J., J. W. Farrell, D. W. Murray, and W. L. Prell (1995), Timescale and paleoceanographic implications of a 3.6 m.y. oxygen isotope record from the northeast Indian Ocean (Ocean Drilling Program Site 758), *Paleoceanography*, *10*, 21–47.

Clemens, S., D. Murray, and W. Prell (1996), Nonstationary phase of the Plio-Pleistocene Asian monsoon, *Science*, *274*, 943–948.

Crowley, T. J. (1995), Ice age terrestrial carbon changes revisited, *Global Biogeochem. Cycles*, *9*, 377–389.

De Deckker, P., and F. X. Gengele (2002), On the occurrence of the giant diatom *Ethmodiscus rex* in an 80–ka record from a deep-sea core, southeast of Sumatra, Indonesia: Implications for tropical paleoceanography, *Mar. Geol.*, *183*, 31–43.

DeMenocal, P. B. (1995), Plio-Pleistocene African climate, *Science*, *270*, 53–59.

Diekmann, B., and G. Kuhn (2002), Sedimentary record of the mid-Pleistocene climate transition in the southeastern South Atlantic (ODP

Site 1090), *Palaeogeogr., Palaeoclimatol., Palaeoecol.*, *182*, 241–258.
Droxler, A., and J. W. Farrell (2000), Marine Isotope Stage 11(MIS 11), New insights for a warm future, *Global Planet. Change*, *24*, 1–5.
Droxler, A., G. A. Haddad, D. A. Mucciarone, and J. L. Cullen (1990), Pliocene-Pleistocene aragonite cyclic variations in Holes 714A and 716B (the Maldives) compared with Hole 633A (the Bahamas): Records of climate-induced $CaCO_3$ preservation at intermediate water depths, *Proc. Ocean Drill. Program Sci. Results*, *115*, 539–577.
Dupont, L. M., B. Donner, R. Schneider, and G. Wefer (2001), Mid-Pleistocene environmental change in tropical Africa began as early as 1.05 Ma, *Geology*, *29*, 195–198.
Emeis, K.-C., H. Doose, A. Mix, and D. Schulz-Bull (1995), Alkenones sea-surface temperatures and carbon burial at Site 846 (eastern equatorial Pacific Ocean): The last 1.3 m.y., *Proc. Ocean Drill. Program Sci. Results*, *138*, 605–613.
Farrell, J. W., and T. R. Janecek (1991), Late Neogene paleoceanography and paleoclimatology of the northeast Indian Ocean (Site 758), *Proc. Ocean Drill. Program Sci. Results*, *121*, 297–355.
Gartner, S. (1988), Paleoceanography of the Mid-Pleistocene, *Mar. Micropaleontol.*, *13*, 23–46.
Gersonde, R., and D. A. Hodell (2002), Southern Ocean paleoceanography—Insights from Ocean Drilling Program Leg 177, *Palaeogeogr. Palaeoclimatol. Palaeoecol.*, *182*, 145–149.
Gingele, F. X., and F. Schmieder (2001), Anomalous South Atlantic lithologies confirm global scale of unusual mid-Pleistocene climate excursion, *Earth Planet. Sci. Lett.*, *186*, 93–101.
Guo, Z., T. Liu, N. Fedoroff, L. Wei, Z. Ding, N. Wu, H. Lu, W. Jiang, and Z. An (1998), Climate extremes in Loess of China coupled with the strength of deep-water formation in the North Atlantic, *Global Planet. Change*, *18*, 113–1228.
Harris, S. E., A. C. Mix, and T. King (1997), Biogenic and terrigenous sedimentation at Ceara Rise, western tropical Atlantic, supports Pliocene-Pleistocene deep-water linkage between hemispheres, *Proc. Ocean Drill. Program Sci. Results*, *154*, 331–345.
Hasselmann, K. (1976), Stochastic climate models: Part I. Theory, *Tellus*, *28*, 473–485.
Haug, G. H., D. M. Sigman, R. Tiedemann, T. F. Pedersen, and M. Sarnthein (1999), Onset of permanent stratification in the Subarctic Pacific Ocean, *Nature*, *401*, 779–782.
Imbrie, J., et al. (1993), On the structure and origin of major glaciation cycles: 2. The 100,000-year cycle, *Paleoceanography*, *8*, 699–735.
Janecek, T. R., and D. K. Rea (1984), Pleistocene fluctuations in Northern Hemisphere trade-winds and westerlies, in *Milankovitch and Climate*, edited by A. Berger et al., pp. 331–347, D. Reidel, Norwell, Mass.
Jansen, J. H. F., A. Kuijpers, and S. R. Troelstra (1986), A Mid-Brunhes climatic event: Long-term changes in global atmosphere and ocean circulation, *Science*, *232*, 619–622.
Keigwin, L. D., and E. A. Boyle (1985), Carbon isotopes in deep-sea benthic foraminifera: Precession and changes in low-latitude biomass, in *The Carbon Cycle and Atmospheric CO_2: Natural Variations Archean to Present*, edited by E. T. Sundquist and W. S. Broecker, pp. 319–328, AGU, Washington, D. C.
Kemp, A. E., R. B. Pearce, I. Koizumi, J. Pike, and S. J. Rance (1999), The role of mat-forming diatoms in the formation of Mediterranean sapropel, *Nature*, *398*, 57–61.
Kucera, M., and J. P. Kennett (2002), Causes and consequences of a middle Pleistocene origin of the modern planktonic foraminifer *Neogloboquadrina pachyderma* sinistral, *Geology*, *30*, 539–542.
Laskar, J. (1990), The chaotic motion of the solar system: A numerical estimate of the size of the chaotic zones, *Icarus*, *88*, 266–291.
Linsley, B. K. (1996), Oxygen-isotope record of sea level and climate variations in the Sulu Sea over the past 150,000 years, *Nature*, *380*, 234–237.
Liu, C., X. Cheng, Y. Zhu, J. Tian, and P. Xia (2002), Oxygen and carbon isotope records of calcareous nannofossils for the past 1 Ma in the southern South China Sea, *Chin. Sci. Bull.*, *47*, 798–803.
Mix, A. C., N. G. Pisias, W. Rugh, J. Wilson, A. Morey, and T. K. Hagelberg (1995), Benthic foraminifer stable isotope record from Site 849 (0–5 Ma): Local and global climate changes, *Proc. Ocean Drill. Program Sci. Results*, *138*, 371–412.
Molfino, B., and A. McIntyre (1990), Precessional forcing of nutricline dynamics in the equatorial Atlantic, *Science*, *249*, 766–769.
Ortiz, J., A. Mix, S. Harris, and S. O'Connell (1999), Diffuse spectral reflectance as a proxy for percent carbonate content in North Atlantic sediments, *Paleoceanography*, *14*, 171–186.
Paul, H. A., J. C. Zachos, B. P. Flower, and A. Tripati (2000), Orbitally induced climate and geochemical variability across the Oligocene/Miocene boundary, *Paleoceanography*, *15*, 471–485.
Pierre, C., P. Belanger, J. F. Saliege, M. J. Urrutiaguer, and A. Murat (1999), Paleoceanography of the western Mediterranean during the Pleistocene: Oxygen and carbon isotope records at Site 975, *Proc. Ocean Drill. Program Sci. Results*, *161*, 481–488.
Prell, W. (1982), Oxygen and carbon isotope stratigraphy for the Quaternary of hole 502B: Evidence for two modes of isotopic variability, *Initial Rep. Deep Sea Drill. Program*, *68*, 455–464.
Raymo, M. E. (1997), The timing of major climate terminations, *Paleoceanography*, *12*, 577–585.
Raymo, M. E., W. F. Ruddiman, J. Backman, B. M. Clement, and D. G. Martinson (1989), Late Pliocene variation in Northern Hemisphere ice sheets and North Atlantic deep water circulation, *Paleoceanography*, *4*, 413–446.
Raymo, M. E., W. F. Ruddiman, N. J. Shackleton, and D. W. Oppo (1990), Evolution of Atlantic-Pacific $\delta^{13}C$ gradients over the last 2.5 m.y., *Earth Planet. Sci. Lett.*, *97*, 353–368.
Raymo, M. E., D. W. Oppo, and W. Curry (1997), The mid-Pleistocene climate transition: A deep sea carbon isotopic perspective, *Paleoceanography*, *12*, 546–559.
Rossignol-Strick, M., M. Paterne, F. C. Bassinot, K.-C. Emeis, and G. J. De Lange (1998), An unusual mid-Pleistocene monsoon period over Africa and Asia., *Nature*, *392*, 269–272.
Ruddiman, W. F., M. E. Raymo, D. G. Martinson, B. M. Clement, and J. Backman (1989), Pleistocene evolution: Northern Hemisphere ice sheets and North Atlantic Ocean, *Paleoceanography*, *4*, 353–412.
Rutherford, S., and S. D'Hondt (2000), Early onset and tropical forcing of 100,000-year Pleistocene glacial cycles, *Nature*, *408*, 72–75.
Sancetta, C. (1999), The mystery of the sapropel, *Nature*, *398*, 27–29.
Sancetta, C., T. Villareal, and P. Falkowski (1991), Massive fluxes of rhizosolenid diatoms: A common occurrence?, *Limnol. Oceanogr.*, *36*, 1452–1457.
Scherer, R., S. Bohaty, D. Harwood, A. Roberts, and M. Taviani (2003), Marine isotope stage 31 (1.07 Ma): An extreme interglacial in the Antarctic nearshore zone, *Geophys. Res. Abstr.*, *5*, 1710.
Schmidt, H., W. H. Berger, T. Bickert, and G. Wefer (1993), Quaternary carbon isotope record of pelagic foraminifers: Site 806, Ontong Java Plateau, *Proc. Ocean Drill. Program Sci. Results*, *130*, 397–409.
Schmieder, F., T. von Dobeneck, and U. Bleil (2000), The Mid-Pleistocene climate transition as documented in the deep South Atlantic Ocean: Initiation, interim state and terminal event, *Earth Planet. Sci. Lett.*, *179*, 539–549.
Schulz, M., and M. Mudelsee (2002), REDFIT: Estimating red-noise spectra directly from unevenly spaced paleoclimatic time series, *Comput. Geosci.*, *28*, 421–426.
Shackleton, N. J. (2000), The 100,000-year ice-age cycle identified and found to lag temperature, carbon dioxide, and orbital eccentricity, *Science*, *289*, 1897–1902.
Shackleton, N. J., A. Berger, and Peltier (1990), An alternative calibration of the lower Pleistocene timescale based on W. R. ODP site 677, *Trans. R. Soc. Edinburgh Earth Sci.*, *81*, 251–261.
Shackleton, N. J., M. A. Hall, and D. Pate (1995), Pliocene stable isotope stratigraphy of Site 846, *Proc. Ocean Drill. Program Sci. Results*, *138*, 337–355.
Shi, Y., X. Liu, B. Li, and T. Yao (1999), A very strong summer monsoon event during the 30–40 ka BP in the Qinhai-Xizang (Tibet) Plateau and its relation to precessional cycle, *Chin. Sci. Bull.*, *44*, 1851–1857.
Shipe, R. F., M. A. Brzezinski, C. Pilskaln, and T. A. Villareal (1999), *Rhizosolenia* mats: An overlooked source of silica production in the open sea, *Limnol. Oceanogr.*, *44*, 1282–1292.
Tian, J., P. Wang, X. Cheng, and Q. Li (2002), Astronomically tuned Plio-Pleistocene benthic $\delta^{18}O$ record from South China Sea and Atlantic-Pacific comparison, *Earth Planet. Sci. Lett.*, *203*, 1015–1029.
Tiedemann, R., M. Sarnthein, and N. J. Shackleton (1994), Astronomic timescale for the Pliocene Atlantic $\delta^{18}O$ and dust flux records from Ocean Drilling Program Site 659, *Paleoceanography*, *9*, 619–638.
Torrence, C., and G. P. Compo (1998), A practical guide to wavelet analysis, *Bull. the Am. Meteorol. Soc.*, *79*, 61–78.
Tréguer, P., D. M. Nelson, A. J. Van Bennekom, D. J. DeMaster, A. Laynaery, and B. Queguiner (1995), The silica balance in the World Ocean: A reestimate, *Science*, *268*, 375–379.
Venz, K. A., and D. A. Hodell (1999), A 1.0 Myr record of Glacial Atlantic Intermediate Water variability from ODP Site 982 in the northeast Atlantic, *Paleoceanography*, *14*, 42–52.
Venz, K. A., and D. A. Hodell (2002), New evidence for changes in Plio-Pleistocene deep

water circulation from Southern Ocean ODP Leg 177 Site 1090, *Palaeogeogr. Palaeoclimatol. Palaeoecol.*, *182*, 197–220.

Villareal, T. A., C. Pilskaln, M. Brzezinski, F. Lipschultz, M. Dennett, and G. B. Gardner (1999), Upward transport of oceanic nitrate by migrating diatom mats, *Nature*, *397*, 423–425.

Wang, P., et al. (2000), *Proceedings of the Ocean Drilling Program Initial Reports* [CD-ROM], vol. 184, Ocean Drill. Program, College Station, Tex.

Wang, P., J. Tian, and X. Cheng (2001), Transition of Quaternary glacial cyclicity in deep-sea records at Nansha, the South China Sea, *Sci. Chin.*, *D44*, 926–933.

Wang, P., J. Tian, X. Cheng, C. Liu, and J. Xu (2003), Carbon reservoir change preceded major ice-sheet expansion at the mid-Brunhes event, *Geology*, *31*, 239–242.

Wehausen, R., and H.-J. Brumsack (1999), Cyclic variations in the chemical composition of eastern Mediterranean Pliocene sediments: A key for understanding sapropel formation, *Mar. Geol.*, *153*, 161–176.

Woodruff, F., and S. M. Savin (1991), Mid-Miocene isotope stratigraphy in the deep sea: High-resolution correlations, paleoclimatic cycles, and sediment preservation, *Paleoceanography*, *6*, 755–806.

Xu, J., P. Wang, B. Huang, Q. Li, and Z. Jian (2004), Response of planktonic foraminifera to glacial cycles: Mid-Pleistocene change in the southern South China Sea, *Mar. Micropaleontol.*, in press.

Yang, L., M. Cheng, R. Wang, and F. Zheng (2002), Radiolarian record to paleoecological environment change events over the past 1.2 Ma BP in the southern South China Sea, *Chin. Sci. Bull.*, *47*, 1478–1483.

Yasuda, M., W. H. Berger, G. Wu, S. Burke, and H. Schmidt (1993), Foraminiferal preservation record for the last million years: Site 805, Ontong Java Plateau, *Proc. Ocean Drill. Program Sci. Results*, *130*, 491–508.

Yu, Z., and Z. Ding (1998), An automatic orbital tuning method for paleoclimate records, *Geophys. Res. Lett.*, *25*, 4525–4528.

Zachos, J., M. Pagani, L. Sloan, E. Thomas, and K. Billups (2001), Trends, rhythms, and aberrations in global climate 65 Ma to present, *Science*, *292*, 686–693.

X. Cheng, C. Liu, J. Tian, P. Wang, and J. Xu, Laboratory of Marine Geology, Tongji University, Shanghai 200092, China. (pxwang@online.sh.cn)